Chemosphere 320 (2023) 138062

Contents lists available at ScienceDirect

Chemosphere

journal homepage: www.elsevier.com/locate/chemosphere

Sorptive removal of phosphorus by flue gas desulfurization gypsum in batch and column systems

Ansley Hamid [a], Alan E. Wilson [a], H. Allen Torbert [b], Dengjun Wang [a,*]

[a] School of Fisheries, Aquaculture and Aquatic Sciences, Auburn University, Auburn, AL, 36849, USA
[b] USDA-ARS National Soil Dynamics Laboratory, Auburn, AL, 36832, USA

HIGHLIGHTS

- FGD gypsum was used to sorb P in batch and flow-through packed column experiments.
- Models were successfully used to simulate P sorption kinetics, isotherms, and transport.
- FGD gypsum showed good capacity in sorbing P from batch and column experiments.
- FGD gypsum shows the potential to remove P from different waters at large scales.

GRAPHICAL ABSTRACT

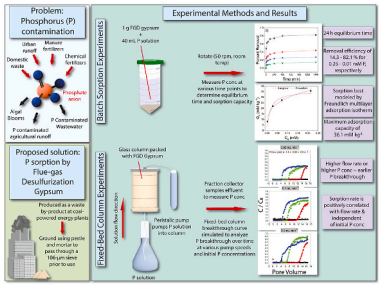

ARTICLE INFO

Handling Editor: Y Yeomin Yoon

Keywords:
Phosphorus
Flue gas desulfurization (FGD) gypsum
Fixed-bed column
Sorption
Removal
Practical application

ABSTRACT

Phosphorus (P) over-loading is often a central topic due to its linkage to harmful algal blooms (HABs) and its importance in wastewater treatment that has fueled immediate remediation attempts to reduce P loading from point (e.g., wastewater) and nonpoint sources (e.g., fertilizers). Conventional remediation techniques (e.g., filtration) are often expensive, ineffective, and difficult to implement at large scales. The flue gas desulfurization (FGD) gypsum produced as an energy plant waste byproduct has recently been advocated as a physiochemical remediation strategy for P through sorptive removal. However, limited research is available on the practical applications of FGD gypsum for P removal from water. Herein, batch sorption experiments were performed to investigate the sorptive removal efficiency of P by FGD gypsum under environmentally relevant P concentrations (0.01–0.25 mM). In parallel, fixed-bed column experiments packed with FGD gypsum were performed using elevated P concentrations (0.1–1.0 mM) to understand the scalability of FGD gypsum for large-scale practical applications. During batch experiments, P sorption equilibrium was reached within 24 h that includes an initially fast step (via boundary layer diffusion), followed by a slow rate-determining step (via intraparticle diffusion). P sorption kinetics followed the pseudo second-order kinetics, indicating chemisorption. P sorption at equilibrium can be simulated by both the Freundlich and Langmuir sorption isotherms. The Langmuir sorption isotherm yielded a maximum sorption capacity (Q_{max}) of 36.1 mM kg^{-1}. The fixed-bed column experimental results showed that sorption rate depends on the applied flow rate, irrespective of the tested P concentrations. Our findings can be extrapolated to evaluate the feasibility and scalability of FGD gypsum in removing P to counteract P runoff and mitigate HABs and P-loaded wastewater.

* Corresponding author.
E-mail address: dzw0065@auburn.edu (D. Wang).

https://doi.org/10.1016/j.chemosphere.2023.138062
Received 2 January 2023; Received in revised form 3 February 2023; Accepted 4 February 2023
Available online 4 February 2023

1. Introduction

As human population and concomitant demands on natural resources explode under a rapidly changing climate, the tasks of managing multitudinous factors to increase global agriculture productivity, while maintaining acceptable water quality become more crucial (Lengnick, 2014). Among these, nutrient, including phosphorus (P) and nitrogen (N) pollution, must be controlled from both point (e.g., wastewater) and nonpoint (e.g., excess chemical and manure fertilization runoff) sources. Also, it is important to consider P in wastewater to reduce P losses, encourage P balance, and increase P utilization efficiency in urban and agricultural settings through recycling P in wastewater. P is often difficult to control in wastewater streams because it occurs in many forms (e.g., particulate, colloidal, and dissolved P with different inorganic and organic species), which requires different strategies for P capturing (Egle et al., 2015). Additionally, P is generally regarded as a limiting nutrient in the environment, prompting farmers to overdose P-containing chemical and animal manure fertilizers to enhance crop yield through bottom-up effects (Boyd and Tucker, 2012; Chislock et al., 2013). P overloading is of particular concern regarding animal manure composts because cattle, swine, and poultry manures are the most important resources of P for crop production (Komiyama and Ito, 2019). Given that P is needed in such a small quantity compared to other major nutrients (Redfield ratio = 106C:16 N:1 P; Redfield, 1958), agricultural P runoff into surface water and loading of high concentrations of P (e.g., >0.7–0.8 mg L^{-1}), coupled with N inputs (>0.6–0.9 mg L^{-1}) from fertilizers, causes eutrophic waters and harmful algal blooms (HABs). HABs are estimated to cause economic costs upwards of $2.2 billion USD per year in the U.S. alone (Chakrabarti, 2018). Therefore, there has been a large push for P removal from various water bodies (Chislock et al., 2013; Dodds et al., 2009; Lehtiniemi et al., 2005).

Common P removal strategies can be categorized into physical (e.g., filtration, aeration, flushing, and dilution), chemical (e.g., precipitation and algaecides for controlling HABs), and biological (e.g., microbial remediation and biomanipulation) techniques (Boyd and Tucker, 2012; van Donk et al., 1990; Zhang et al., 2020). Nonetheless, none has been demonstrated cost-effective, efficient, and sustainable. Algaecides, such as copper sulfate ($CuSO_4$), can effectively reduce HABs temporarily (Buley et al., 2021). However, $CuSO_4$ is relatively expensive and potentially harmful to nontarget organisms, which may cause secondary long-term pollution once these algae are killed off (Boyd and Tucker, 2012; Buley et al., 2021; Chislock et al., 2013). Physical strategies are typically only effective for small-scale water bodies that require a plentiful volume of good quality water to dilute the pollution (Zhang et al., 2020). The efficiency of biological methods is largely impacted by various environmental factors (e.g., temperature and sunlight) and nontarget organisms (van Donk et al., 1990; Zhang et al., 2020). There has not been a holistically successful approach to effectively control P in recreational and drinking water bodies and wastewater. To this end, there is a strong need to approach a cost-effective, environmentally friendly, and more sustainable strategy in combatting P pollution and HABs.

Gypsum can be used as a physiochemical approach for P remediation via physical and chemical sorption. Gypsum occurs ubiquitously in nature as the modestly soluble salt form of calcium sulfate ($CaSO_4{\cdot}2H_2O$). Gypsum can also be produced as a waste byproduct at coal-powered energy plants (Gypsum Association, 2022). Calcium sulfite is created in limestone oxidation scrubbers that remove sulfur dioxide (SO_2) from the flue gas stream after coal combustion is oxidized into flue gas desulfurization (FGD) gypsum (Gypsum Association, 2022). It is estimated that, of 12 million tons of FGD gypsum produced in 2016, approximately 25% was landfilled (U.S. EPA, 2008). FGD gypsum production reached an all-time high of 20.7 million tons in 2017 (Crangle, 2021). It is anticipated that the FGD gypsum market will be valued at approximately $1.1 billion USD by 2028, growing at a compounded annual growth rate of 5.6% from 2021 to 2028 (CDN Newswire, 2022). For this reason, it is highly beneficial to explore how and to what extent FGD gypsum can be used to remove P, since it is considered as a waste byproduct with an increasing market size that would otherwise contribute to a global landfill crisis.

Documented research on the potential use of FGD gypsum for P immobilization has primarily focused on soil systems. For example, ~13% gypsum addition into the Ghanimeh soil, coupled with increasing soil pH from 5.6 to 7.5, was found to increase P sorption capacity from 1750 μg g^{-1} to 2600 μg g^{-1} (Kordlaghari and Rowell, 2006). However, very limited research has been conducted on the use of FGD gypsum for P removal in aqueous solutions (He et al., 2018; Torbert and Watts, 2014). Higgins et al. (1976) found that, when 500 mg L^{-1} gypsum was added to a lake, the lake water pH was increased from 7 to 10 and the dissolved orthophosphate (PO_4^{3-}) concentration was reduced from 400 to ~40 μg L^{-1}. This corresponds to a 90% removal efficiency of P compared to neutral pH condition. Similarly, Ma et al. (2023) reported that, at an applied FGD gypsum concentration of 3.44 g L^{-1}, a maximum P removal efficiency of ~87% was achieved when solution pH ranged 8.5–9.0. The enhanced P sorption at high pH is likely due to the formation of hydroxyapatite precipitates ($Ca_{10}(PO_4)_6(OH)_2$) that are favorably produced between calcium (Ca^{2+}) from gypsum and phosphate (PO_4^{3-}) at high pH conditions (rich in OH^- ions) (Kordlaghari and Rowell, 2006). However, the lack of systematic investigations on the potential use of FGD gypsum in aquatic environments for P removal under environmentally relevant conditions, prompts the need of more extensive studies on its usability to better understand its scalability in agricultural and urban systems.

Gypsum application in agriculture has shown multiple benefits, including a reduction in soil crusting, HABs, chemical oxygen demand (COD), organic matter concentration, off-flavor fish substances, and total alkalinity, while increasing plant nutrient availability and dissolved oxygen content (Chen and Warren, 2011; Dontsova et al., 2005; Wu and Boyd, 1990). Particularly, Watts and Dick (2014) predicted that, even when applied at a rate (i.e., 170 Mg/ha) representing cumulative 80-year application, FGD gypsums will still exhibit positive environmental impacts primarily. Therefore, gypsum may provide a cost-competitive, more effective strategy to mitigate P pollution than previously implemented techniques, while supporting crucial aspects of soil and water chemistry. In this research, batch sorption experiments were performed to determine the sorption efficiency and mechanisms of P by FGD gypsum under environmentally relevant P concentrations (0.01–0.25 mM). The novelty of this research lies in the fixed-bed gypsum column experiments performed using elevated P concentrations (0.1–1.0 mM) to understand the feasibility and scalability of gypsum in practical applications. Our findings shed light on the use of FGD gypsum as a sustainable means for P removal from water (e.g., HABs, fertilizer runoff, and wastewater treatment plant effluents).

2. Materials and methods

2.1. FGD gypsum and phosphorus sample preparation

The as-received FGD gypsum was ground by pestle and mortar, and then passed through a 106-μm sieve, so all FGD gypsum used was <106-μm in size. Phosphorus stock solutions were prepared using reagent grade NaH_2PO_4 (J.T. Baker) in the following concentrations: 0.01, 0.05, 0.10, 0.25, 0.50, 1.0, 2.5, 5.0, and 10 mM. Phosphorus stock solutions ranging from 0.01 to 1.0 mM P were used for kinetics, batch sorption, and fixed-bed column experiments (shown below). Higher P stock solutions of 2.5–10 mM were also included for gypsum characterization to understand general pH and zeta potential changes versus P concentrations.

2.2. Characterization of the FGD gypsum

The mineralogical characteristics of the FGD gypsum were

characterized using X-Ray diffraction (XRD) (AXRD powder diffraction system, Proto Manufacturing, U.S.) with a Cu radiation source at 2.2° min^{-1} and a scanning range from 10 to 100° (40 kV tube voltage at 30 mA current). The surface functional groups of FGD gypsum were analyzed using Fourier-transform infrared (FT-IR) spectroscopy (FTIR-6800, JASCO) with a KBr blank and a 4000–600 cm^{-1} spectral range at 2 mm s^{-1}. To better understand the physiochemical properties of FGD gypsum after P sorption, 1.0 g of FGD gypsum was added to 40 mL of P solutions with varying concentrations (0, 0.10, 0.25, 0.50, 1.0, 2.5, 5.0, and 10 mM) in a 50 mL centrifuge tube (pH was not adjusted to observe the effect of increasing P concentration on solution pH). The pH of these solutions was measured on an Orion Star A210 pH meter (Thermo Scientific). Afterwards, 1 mL aliquot was sampled from each tube to determine zeta potential (surface charge) of FGD gypsum under different P concentrations on a Malvern Panalytical Zetasizer Pro Blue analyzer (Malvern, U.K.). After washing the DTS 1070 folded capillary cell by five times with 95% ethanol (VWR), 1 mL sample was halfway injected invertedly and then upright with a syringe to remove any air bubbles. The zeta potential was then measured on the Zetasizer Pro Blue at 25 °C with a 120 s equilibrium time for 10–100 runs. All pH and zeta potential measurements were conducted in triplicate.

2.3. Kinetics and batch sorption experiments of phosphorus by FGD gypsum

To determine the equilibrium time and removal mechanisms of P by the FGD gypsum, batch sorption experiments were performed in triplicate at room temperature (25 °C) without pH adjustment. Briefly, 1.0 g of FGD gypsum was weighted into a 50 mL centrifuge tube with 40 mL of P solution (0, 0.01, 0.05, 0.10, and 0.25 mM). These environmentally relevant P concentrations were utilized, since the standard curve of this P concentration range measured by the UV-VIS spectrophotometer (Lambda 365, PerkinElmer) has a high linearity with $r^2 > 0.99$. The solutions were shaken on a tissue rotator (Thermo Scientific) at a speed of 50 rpm at room temperature (25 °C). A 5 mL aliquot of sample solution was taken in the following time intervals: 10 min, 30 min, 1 h, 2 h, 4 h, 8 h, and 24 h. Afterwards, each sample was centrifuged (Allegra X-30R Centrifuge, Beckman Coulter, U.S.) at 3600 rpm for 30 min, and the supernatant was filtered through a 0.45 μm syringe filter. The P concentration in the filtrate was determined using the molybdate blue method on the PerkinElmer Lambda 365 UV-VIS Spectrophotometer at 881 nm (Murphy and Riley, 1962). This P concentration was then compared to the initial P concentration to determine the amount of sorption that occurred at each time interval during the experiment.

Analyzing P concentrations at various sampling times enabled us to determine at what time the P sorption by FGD gypsum reached equilibrium. This also indicated the time at which FGD gypsum became completely saturated with P. Data was simulated using the pseudo first-order kinetics and pseudo second-order kinetics models on Origin software. The equations for the pseudo first- and second-order kinetics were given in Eq. (1) and Eq. (2), respectively. The intraparticle diffusion model was also used for P sorption by FGD gypsum to understand the rate-determining step of the sorption process. The Weber and Morris (1963) model for exploring intraparticle diffusion was shown in Eq. (3).

$$\mathrm{Ln}(Q_e - Q_t) = \mathrm{Ln}\, Q_e - k_1 * t \tag{1}$$

$$\frac{t}{Q_t} = \left(\frac{1}{k_2 * Q_e^{\,2}}\right) + \frac{t}{Q_e} \tag{2}$$

$$Q_t = k_{id}\sqrt{t} \tag{3}$$

where Q_e is the sorbed amount of P by the FGD gypsum at equilibrium (mM kg^{-1}); Q_t is the sorbed amount at time t; k_1 and k_2 are the reaction rate constants for the pseudo first- and second-order kinetics, respectively (kg mM^{-1} min^{-1}); and k_{id} is the intraparticle diffusion constant (mM kg^{-1} $min^{-1/2}$).

The sorption isotherms were fitted by the Langmuir and Freundlich models on Origin. The Langmuir and Freundlich models were shown in Eq. (4) and Eq. (5), respectively.

$$Q_e = Q_{max} * b * \left(\frac{C_e}{1 + b * C_e}\right) \tag{4}$$

$$Q_e = K * C_e^{\frac{1}{n}} \tag{5}$$

where Q_{max} is the max sorption capacity (mM kg^{-1}), C_e is the concentration at equilibrium (mM), and b_L and K_f are the Langmuir and Freundlich constants, respectively.

2.4. Fixed-bed column experiments

Maximum sorption capacity was further explored using fixed-bed column experiments in duplicate with higher P concentrations (0.1–1.0 mM) than those used in the batch sorption experiments. A fixed-bed column sorption experiment is advantageous in this scenario because of its feasible design allowing for high removal efficiencies and scalability to practical applications, notably to higher concentrations of P in wastewater and industrial use compared to batch sorption experiments (Cavalcante, 2000; Patel, 2019; U.S. EPA, 1983). A glass chromatography column with an inner diameter of 1.7 cm and length of 10 cm (Wang et al., 2015, 2017, 2018) was dry packed with the ground and sieved FGD gypsum (<106-μm). Both inlet and outlet ends of the column were lined with a 45-μm nylon mesh filter to prevent potential release of the FGD gypsum with introduced flow. The packed column was then slowly saturated with ultrapure water in an upward mode using a peristaltic pump (LongerPump YZ1515x, China) to determine its pore volume and porosity. After the completion of the saturation step, a NaH_2PO_4 solution at 0.10, 0.25, 0.50, or 1.0 mM was injected into the column in an upward mode at three environmentally relevant flow rates (0.05, 0.10, and 0.60 mL min^{-1}, respectively). The fixed-bed column experiments were conducted at room temperature (25 °C) without pH adjustment. These low flow rates were chosen since maximum saturation and sorption are two targeted parameters. Literature has shown that significantly higher saturation of breakthrough time and higher adsorbate removal occurred at lower flow rates due to increased contact time (residence time) in the column (Ahmad and Hameed, 2010; Patel, 2019; Sheng et al., 2018). The column effluent was collected on a fraction collector (Huxi BSZ-100 Automatic Fraction Collector, China) at specified time increments based on the pore volume and flow rate. The P concentration of column effluent was determined using the method described previously on the UV-VIS spectrophotometer. The data were then extrapolated in Origin to visualize the breakthrough curve (BTC) of P over the number of pore volumes of P injected into the column.

Due to very limited results reported on P sorption by FGD gypsum in fixed-bed columns, a wide range of models were utilized to analyze the BTC data. The BTC data were simulated by linear regression using the following five sorption performance models shown in Equations (6)–(10), respectively: Thomas; Adams-Bohart; Clark; Yoon-Nelson; and Yan models. The Thomas model is one of the commonly used column performance models. It assumes Langmuir adsorption and pseudo second-order kinetics that requires the maximum sorption of an adsorbent (Huang et al., 2022; Thomas, 1944). The Adams-Bohart model is applied to the initial stage of the BTC and assumes a step isotherm with a constant adsorbent capacity (Bohart and Adams, 1920; Chiavola et al., 2012; Huang et al., 2022). The Clark model is based on mass transfer concept and the Freundlich isotherm to simulate the BTC through a generalized logistic function (Clark, 1987; Huang et al., 2022). The Yoon-Nelson model is a simplistic function, assuming the rate of decrease in sorption probability is proportional to sorptive breakthrough probability, which requires limited data concerning adsorbate characteristics or physical properties of the sorption bed (Huang et al., 2022;

Yoon and Nelson, 1984; Zhang et al., 2011). Lastly, the Yan model was recently developed that assumes multiple rate-limiting steps during sorption to minimize errors resulting from the Thomas model (de Franco, 2017; Huang et al., 2022; Yan et al., 2001).

The Thomas Model:

$$\mathrm{Ln}\left(\frac{C}{C_0}\right) = \left(\frac{k_T * q * m}{Q}\right) - k * C_0 * t \quad (6)$$

where k_T is the Thomas rate constant (mM^{-1} min^{-1}), q is the maximum solid-phase concentration of the sorptive species at equilibrium (mM mL g^{-1}), and m is the mass of sorbent (g). The parameters k_T and q can be determined by a plot of $\ln\left(\frac{C_0}{C} - 1\right)$ vs. t.

The Adams-Bohart Model:

$$\mathrm{Ln}\left(\frac{C}{C_0}\right) = k_{AB} * C_0 * t - \frac{k_{AB} * N_0 * z}{u_0} \quad (7)$$

where k_{AB} is the Adams-Bohart rate constant (mM^{-1} min^{-1}), N_0 is the sorbed amount at equilibrium (mM), z is the bed depth (cm), and u_0 is the superficial flow rate (cm min^{-1}). The parameters k_{AB} and N_0 can be determined by a plot of $\ln\left(\frac{C_0}{C} - 1\right)$ vs. t.

The Clark Model:

$$\mathrm{Ln}\left(\left(\frac{C_0}{C}\right)^{n-1} - 1\right) = \mathrm{Ln}\, A - k_C * t \quad (8)$$

where A is the Clark model constant (−), k_C is the sorption rate (−) and n is the Freundlich isotherm constant (determined in this experiment). The parameters A and k_C can be determined by a plot of $\ln\left(\left(\frac{C_0}{C}\right)^{n-1} - 1\right)$ vs. t.

The Yoon-Nelson Model:

$$\mathrm{Ln}\left(\frac{C_t}{C_0 - C_t}\right) = k_{YN} * t - k_{YN} * \tau \quad (9)$$

where k_{YN} is the rate constant (min^{-1}), τ is the time required for 50% adsorbate breakthrough (min), and t is the time. The parameters k_{YN} and τ can be determined by a plot of $\ln\left(\frac{C}{C_0 - C}\right)$ vs. t.

The Yan Model:

$$\mathrm{Ln}\left(\frac{C_t}{C_0 - C_t}\right) = \frac{k_{Yan} * C_0}{Q}\mathrm{Ln}\left(\frac{Q^2}{k_{Yan} * Q_e * m}\right) + \left(\frac{k_{Yan} * C_0}{Q}\right)\mathrm{Ln}\,(t) \quad (10)$$

where k_{Yan} is the Yan model constant (−), Q_e is the amount of P sorbed onto gypsum at equilibrium (mM g^{-1}), m is the mass of gypsum (g), and Q is the volumetric flow rate (mL min^{-1}). The parameters k_{Yan} and Q_e can be determined by a plot of $\ln\left(\frac{C}{C_0 - C}\right)$ vs. Ln (t).

2.5. Statistical analysis

A one-way ANOVA was performed using R software to determine if there is a significant difference at the $p < 0.05$ level for the collected data (e.g., zeta potential and P sorption capacity).

3. Results and discussion

3.1. FGD gypsum and phosphorus characterization

The physicochemical properties of the FGD gypsum and conventional gypsum (mined natural gypsum, as a comparison) were summarized in the Supplementary Information Tables S1 and S2. The FGD gypsum had a higher purity and water content, typically with lower amounts of macronutrients, micronutrients, and elements of environmental concern (e.g., toxic heavy metals). Notably, the FGD gypsum contained <1 mg L^{-1} P compared to that of mined natural gypsum (~30 mg L^{-1}), which may play an important role in impacting the removal efficiency of P by gypsum.

The FT-IR (Fig. 1a) and XRD (Fig. 1b) were used to analyze the composition and purity of the FGD gypsum. Table S3 showed the most characteristic FT-IR bands of the FGD gypsum reported in the literature. The doublet at 3554 cm^{-1} and 3405 cm^{-1} with a weak shoulder at 3243 cm^{-1} was assigned for O–H stretching. Peaks at 1685 cm^{-1} and 1620 cm^{-1} corresponded to the H–*O*–H bending vibrations from loosely- and strongly-holding water, respectively. The strong peak at 1115 cm^{-1} with the weak shoulder at 1142 cm^{-1} represented SO_4^{2-}, while the weak peak at 669 cm^{-1} was consistent with OS-O bending vibrations. The XRD spectrum for FGD gypsum with reflections at $2\theta = 11.67°$, 20.75°, 29.15°, 31.15°, 33.41°, and 43.39° was coincided with those in the literature, with no indication of quartz or dolomite in the sample (Cheng et al., 2018; Kamitsou et al., 2020; Koukouzas and Vasilatos, 2008). Both FT-IR and XRD spectra confirmed a high purity of the FGD gypsum used in this study.

The pH and zeta potential of gypsum suspensions with and without P at different concentrations (0, 0.10, 0.25, 0.50, 1.0, 2.5, 5.0, and 10 mM) were shown in Fig. 2. The statistical analysis results (ANOVA) showed that pH and zeta potential values were both independently significantly different ($p < 0.05$) under different P concentrations. Because the P stock solution (NaH_2PO_4) was acidic (pH = 5.5–4.7 for the P concentrations ranging 0.1–10 mM), adding higher P concentration into the FGD gypsum solution caused a decrease in solution pH. One exception is that the pH was increased when the P concentration was increased from 0.25 to 0.50 mM. Increasing P concentration resulted in a decrease in zeta potential, due to the enhanced sorption of negatively charged PO_4^{3-} ions. An exception of this trend occurred between P concentration of 0 mM and 0.50 mM, in which the zeta potential was increased and then decreased. These pH and zeta potential results may be due to: 1) lower P concentrations in solution with varying solution chemistry, and 2) chemical heterogeneity on the FGD gypsum surface at higher P concentrations in the solution. For this reason, it is needed to investigate pH and zeta potential trends at higher P concentrations, notably up to 10 mM P.

3.2. Sorption kinetics

To determine the sorptive kinetics of P by the FGD gypsum, batch sorption experiments were performed and analyzed at various time points (Fig. 3a). The sorption of P increased quickly during the early phase (0–60 min), and then increased slowly until the sorption equilibrium was reached (at ~24 h). These findings suggest that there are two types of sorption kinetics (fast and slow sorption processes) with different sorption mechanisms that are reflected by k_{id1} and k_{id2}, respectively. This is verified by the intraparticle diffusion plot shown in Fig. 3b.

The model-fitted parameters for particle diffusion are shown in Table 1. The particle diffusion plot showed that each dataset did not perfectly follow one linear trend and that the data did not pass through the plot origin (0, 0). There is evidence of a two-stage linear relationship with an initially steeper slope during the early phase, followed by a less steep slope as the sorption approaches equilibrium. This is confirmed by a higher k_{id1} value than the k_{id2} value during the early phase sorption, indicating a faster initial rate step. The initial rapid sorption phase likely suggests boundary layer diffusion of P until active sorption sites are completely occupied. Afterwards, the slower, rate-limiting intraparticle diffusion step starts to dominate, indicating irreversible chemisorption (de Franco, 2017; Huang et al., 2022). The values of the sorption rate constants also increased for both the fast and slow sorption step with increasing initial P concentration. These indicate a longer time required to reach equilibrium at higher initial P concentrations. Sorption appears to be limited by P concentration, as intraparticle diffusion is more limiting at lower P concentrations where extremely low P

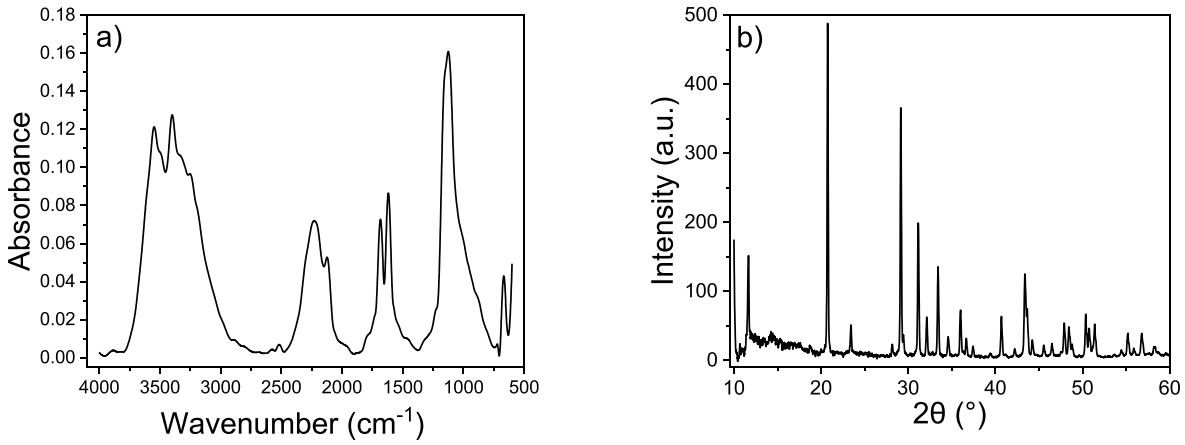

Fig. 1. a) Fourier-transform infrared (FT-IR), and **b)** X-ray diffraction (XRD) spectra of the FGD gypsum used in this study.

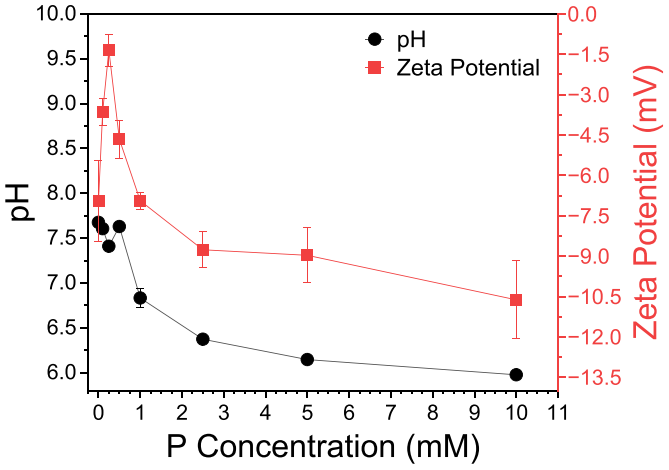

Fig. 2. The pH and zeta potential of gypsum suspensions (1.0 g/L) at different P concentrations (0, 0.10, 0.25, 0.50, 1.0, 2.5, 5.0, and 10 mM). The error bars represent the standard deviations of triplicate experiments.

concentrations are present in solution. Rates of P sorption could also be affected by P particle size, affinity of FGD gypsum for P, and/or pore-size distribution (FGD gypsum pores are likely present at higher calcination temperatures) (Cheng et al., 2018).

The model-fitted results by the pseudo first-order and second-order kinetics models on P sorption by the FGD gypsum were shown in Fig. 4a–b and Table 1. Clearly, P sorption by the FGD gypsum can be better described by the pseudo second-order kinetics model ($R^2 = 1$)

Table 1
Kinetic parameters determined by the pseudo first-order and second-order kinetic models and the intraparticle diffusion model.

Parameters	C_0 (mM)			
	0.01	0.05	0.10	0.25
Pseudo first-order kinetics				
k_1 (kg mM^{-1} min^{-1})	−0.124	−0.0489	−0.0385	−0.0307
Ln (Q_e)	1.52	0.845	0.719	0.861
R^2	0.83	0.79	0.83	0.86
Pseudo second-order kinetics				
k_2 (kg mM^{-1} min^{-1})	36.0	356	725	101,3
Q_e (mM kg^{-1})	8.28	22.3	27.8	36.6
R^2	1.00	1.00	1.00	1.00
Intraparticle diffusion				
k_{id1} (mM kg^{-1} min$^{-1/2}$)	0.312	0.167	0.0602	0.117
Intercept (mM kg^{-1})	4.00	10.1	12.2	15.4
R^2	0.89	0.99	0.99	0.96
k_{id2} (mM kg^{-1} mi$^{-1/2}$)	0.024	0.151	0.174	0.362
Intercept (mM kg^{-1})	7.31	16.4	21.1	22.7
R^2	0.51	0.94	0.85	0.89
Q_e (mM kg^{-1})	8.21	22.0	27.4	35.7
Removal efficiency (%)	82.1	44.0	27.4	14.3

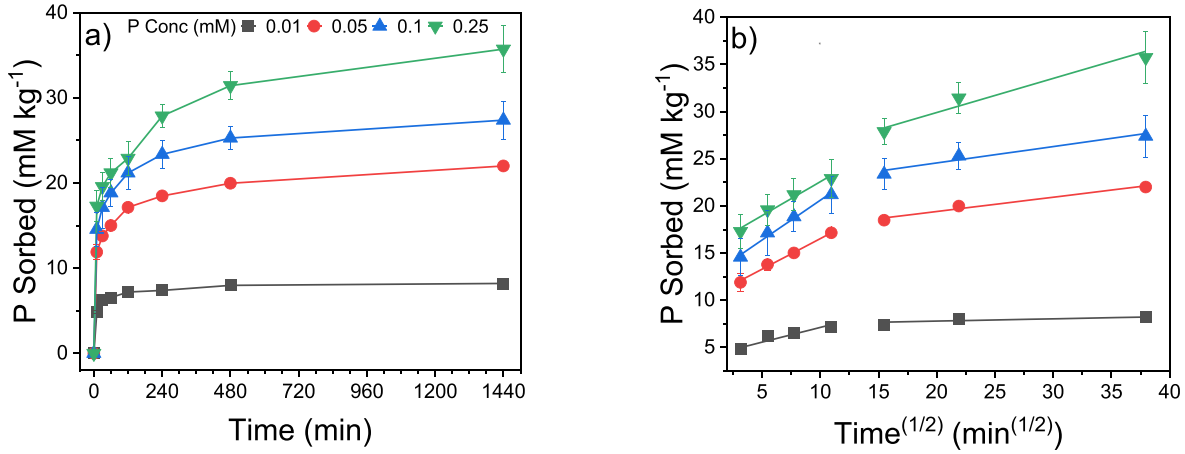

Fig. 3. a) Sorption of P by FGD gypsum versus time after 1.0 g gypsum was added into a 40 mL of P solution (0–0.25 mM). **b)** Intraparticle diffusion plot modeled by Weber and Morris (1963), in which the linear best fit is portrayed by the solid line. Split solid lines represent a distinction between separate rate-determining steps until equilibrium is reached. The error bars represent the standard deviations in triplicate experiments.

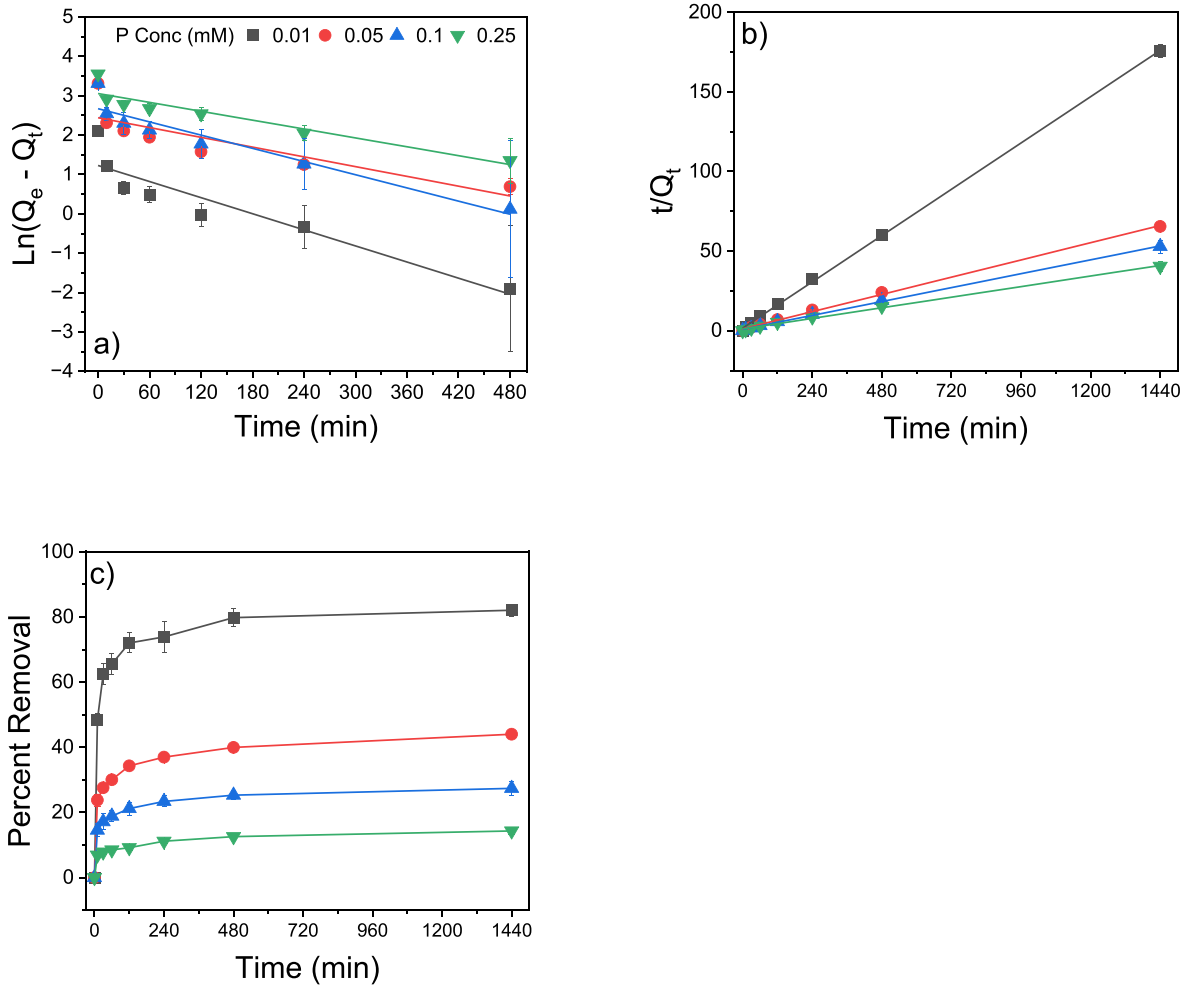

Fig. 4. Sorption of P by FGD gypsum versus time after 1.0 g gypsum was added into a 40 mL of P solution (0–0.25 mM). The error bars represent the standard deviations in triplicate experiments. **a)** pseudo first-order kinetics model simulation; **b)** pseudo second-order kinetics model simulation; and **c)** removal efficiency (%) of P with respect to initial P concentration versus time.

than the pseudo first-order kinetics model (mean $R^2 = 0.83$). This implies that P sorption by FGD gypsum is better explained by chemical reactions between FGD gypsum surface and P (assumptions in the pseudo second-order kinetics model), rather than physical reactions such as van der Waals forces, hydrogen bonding, and electrostatic interactions (in the pseudo first-order kinetics model). Chemical reactions also indicate a stronger bond strength between FGD gypsum and P than physical reactions. The reaction rate constant for pseudo second-order kinetics increases with increasing starting P concentration, which is expected as active sites become saturated faster at higher initial P concentrations. The removal efficiency (%) of P over time at each P concentration was shown in Fig. 4c, and the total removal efficiency (%) is shown in Table 1. The removal efficiency ranged from 82.1% to 14.3%, when the P concentration was increased from 0.01 mM to 0.25 mM. Given that the overall P sorption sites onto FGD gypsum are fixed, the removal efficiency (%) was lower at a higher P concentration. The amount of P sorbed by gypsum at equilibrium was also shown in Table 1. The one-way ANOVA results show that the sorbed amount of P at equilibrium is significantly different ($p < 0.05$) based on the initial P concentration. The amount of P sorbed at equilibrium in reference to the amount of FGD gypsum present increases with increasing P concentration, since there is more competition for active sites on FGD gypsum surface. At the lowest starting P concentration of 0.01 mM, 8.21 mM kg^{-1} was sorbed. When the starting P concentration was increased to 0.25 mM, the sorbed P was increased to 35.7 mM kg^{-1}.

It is important to note that the equilibrium of P sorption by FGD gypsum at the solid: solution ratio of 1: 40 (1 g gypsum in 40 mL solution) was reached at 24 h. Previous studies showed that equilibrium at similar gypsum: P ratios was reached at 1–2 h, in which the utilized gypsum was calcined at various temperatures (Cheng et al., 2018). Experiments with iron oxide-coated gypsum compounds reported a shorter equilibrium time at 15 min (Bastin et al., 1999). This is likely due to the strong interaction between P and iron oxide, resulting in a faster sorption kinetics. For practical application, the equilibrium time by using our FGD gypsum can be shortened with a more vigorous mixing strategy, higher gypsum concentration, or under different environmental conditions (e.g., temperature and pH) that favor the fast sorption between P and FGD gypsum.

Depending on the P concentration, our FGD gypsum can remove 14.3–82.1% P from water (Fig. 4c). These P removal efficiencies were similar to those reported in the literature on P removal by other gypsums or gypsum related compounds. For example, ~23–67% reduction in P concentrations compared to untreated lake water with a P concentration of 600 mg L^{-1} was observed with varying analytical grade gypsums at 100–500 mg L^{-1} (Higgins et al., 1976). Higgins et al. (1976) also suggested that the sorption of P by gypsum was most efficient at higher pH conditions (e.g., above pH 10 resulted in a 90% reduction in P). Similar results were found when pH of gypsum-containing soils was increased from natural pH conditions (3.6–5.5) to a pH of 6.5 and 7.5 (Kordlaghari and Rowell, 2006). Compared to P removal of drainage water via gypsum bed filtration, the current research is roughly similar. Bryant et al. (2012) found a 9.2% P removal in storm flow taking base flow into

account and a 17–30% P removal efficiency with the use of an improved gypsum bed filtration system. This suggests that our batch sorption test of P by FGD gypsum is consistent with literature using gypsum-related compounds and is likely more efficient at alkaline pH conditions.

3.3. Sorption isotherms

The Langmuir and Freundlich sorption isotherms of P by FGD gypsum were shown in Fig. S1, with model-fitted parameters showing in Table S4. The Freundlich isotherm model ($R^2 = 0.98$) performed better ($R^2 = 0.88$) for P sorption by the FGD gypsum. This implies multilayer sorption of P onto FGD gypsum surface rather than monolayer sorption. This also indicates that sorbed P molecules likely interact with each other on the FGD gypsum surface, resulting in a stronger FGD gypsum-P bond. The Langmuir simulated maximum sorption capacity (Q_{max}) is 36.1 mM kg^{-1}, which is similar to the previously determined Q_e (35.7 mM kg^{-1}) when P concentration was 0.25 mM. These findings suggest that, at these higher P concentrations of 0.25 mM with a 25 g L^{-1} gypsum, P removal efficiency will likely remain around 14%. Increasing the FGD gypsum concentration could allow for a greater P sorptive removal. Limited research has been conducted on sorption isotherms of P by FGD gypsum; however, one study suggested that the removal efficiency of gypsum can be significantly improved by treating the gypsum via calcination at different temperatures. Specifically, Cheng et al. (2018) found that Q_{max} was increased by 67% when FGD gypsum was calcined at 600 °C compared to raw FGD gypsum. This is because calcining FGD gypsum at 600 °C can significantly increase the amount of active Ca sites and thus provide a reactive alkaline environment when FGD is decomposed (Cheng et al., 2018). Table S5 summarized the maximum sorption capacity (Q_{max}) of P by our FGD gypsum and other sorbents under similar environmental conditions (25 °C without pH manipulation) in the literature. Our FGD gypsum performed roughly similar to activated alumina, and its P sorption capacity was at least 2-folds higher than that of expanded clay (Filtralite-P™), fly ash, limestone, sand, and zeolite (Johansson, 1999; Klimeski et al., 2014; Wang et al., 2009; Zhang et al., 2018). Overall, our FGD gypsum showed a higher Q_{max} than 60% of the other reported sorbents in Table S5.

3.4. Fixed-bed column experiments

To further explore maximum sorption capacity, the fixed-bed column experiments were performed at various flow rates with a range of initial P concentrations. A P solution at 0.1, 0.25, 0.50, or 1.0 mM was injected into the column at three flow rates (0.05, 0.10, and 0.60 mL min^{-1}, respectively). The column breakthrough curve (BTC) was obtained by plotting the pore volume versus the normalized breakthrough concentration (C/C_0), where C is the column effluent P concentration at time t and C_0 is the initial P concentration (Fig. 5). No breakthrough was observed at the lowest P concentration of 0.10 mM, indicating that the maximum sorption capacity of gypsum was not reached. For this reason, the 0.1 mM P concentration was disregarded from modeling (data cannot be simulated since all data are 0). The slope of the BTC becomes steeper with increasing flow rate, indicating a slower sorption kinetics at higher flow rates. It is apparent that higher initial concentrations of P result in earlier breakthrough. For instance, at a flow rate of 0.05 mL min^{-1}, the initial breakthrough of P was shortened from 13 PV to 8 PV, and then to 4 PV when the P concentration was increased from 0.25 mM to 0.5 mM, and then to 1 mM P, respectively. A similar trend was obtained at the other flow rates (0.10 and 0.60 mL min^{-1}). These findings are consistent with those from the kinetics experiments (Fig. 4b), where a higher initial P concentration corresponds to a higher pseudo second-order rate constant (k_2) and a faster reaction speed.

The Thomas, Adams-Bohart, Clark, Yoon-Nelson, and Yan models were employed to evaluate the dynamic fixed-bed performance of FGD gypsum under various initial P concentrations and flow rates. The fitted parameters and associated R^2 values are shown in Table 2. The Thomas model has the best overall performance, showing the highest average R^2 value of 0.967. The Thomas, Adams-Bohart, Clark, and Yoon-Nelson show similar trends that the rate constant (k) value increases with increasing flow rate. However, no clear trend across all models was observed between the rate constant (k) and initial P concentration. This likely indicates that a faster sorption of P occurs with increasing flow rate, but may be irrespective of the P concentration. These models also show that there is no relationship between sorption capacity (or sorption amount) at equilibrium with flow rate or initial P concentration. For example, in the Thomas model, the Q_e value does not show trends with respect to flow rate or initial P concentration, suggesting that the maximum sorption of P is not dependent on flow rate or initial P concentration. The Yan model confirms this, as the sorbed amount of P at equilibrium does not show trends with respect to flow rate or initial P concentration. Additionally, the Yoon-Nelson model determines that the time required for 50% P breakthrough (compared to the initial P concentration) decreases with increasing flow rate and initial P concentration. This indicates that the saturation of the column occurs more rapidly under these conditions. This is consistent with previous findings from Fig. 5 that higher flow rates correlate to earlier P breakthrough and that higher initial P concentrations result in steeper BTC slopes.

It is important to note that the kinetics, batch sorption, and fixed-bed column experiments all provided similarly comparable results. These findings can be compiled to provide important insights regarding P sorption by FGD gypsum and practical usability at large scale (e.g., runoff and water/wastewater treatment). The kinetics experimental

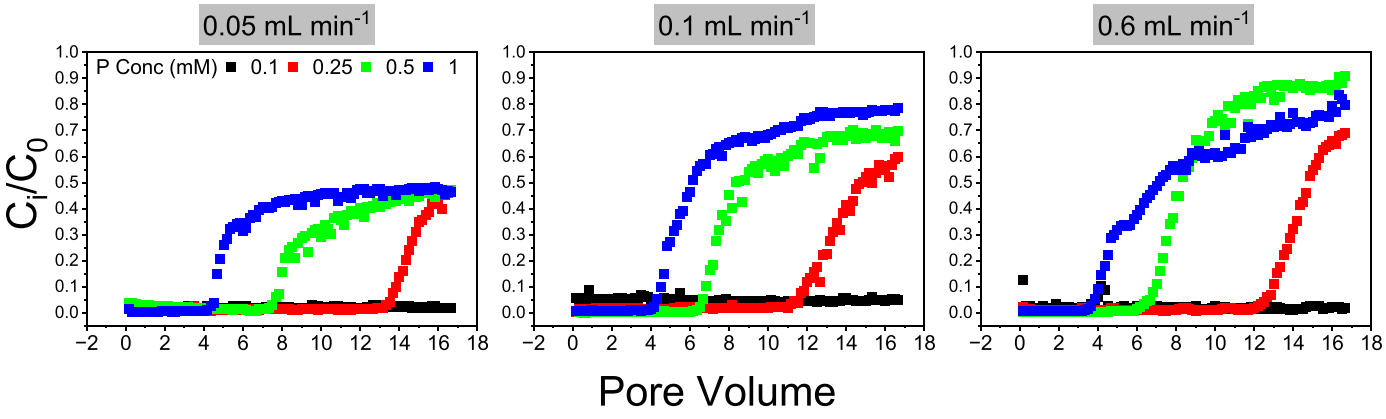

Fig. 5. Column breakthrough curve (BTC) after 16 pore volumes of P solutions at 0.10, 0.25, 0.50, and 1.0 mM were injected into the column packed with FGD gypsum at three different flow rates (0.05, 0.10, and 0.60 mL min^{-1}). Data represents the average C_i/C_0 between duplicate experiments where C_i and C_0 refer to the concentrations of P in column effluents at time i and time 0.

Table 2
Fitted parameters of fixed-bed column models at different P concentrations and flow rates.

Thomas	C_0 (mM)	Q (mL min^{-1})	k_T (mM^{-1} min^{-1})	q (mM mL g^{-1})	R^2
	0.25	0.05	0.068	1.10	0.994
	0.25	0.10	0.048	1.04	0.914
	0.25	0.60	0.062	10.2	0.996
	0.50	0.05	0.001	2.63	0.848
	0.50	0.10	0.112	1.07	0.992
	0.50	0.60	0.347	1.15	0.993
	1.0	0.05	0.031	1.54	0.974
	1.0	0.10	0.055	1.47	0.992
	1.0	0.60	0.293	1.34	0.996
Adams-Bohart	C_0 (mM)	Q (mL min^{-1})	k_{AB} (mM^{-1} min^{-1})	N_0 (mM)	R^2
	0.25	0.05	0.040	1.27	0.986
	0.25	0.10	0.036	1.21	0.901
	0.25	0.60	0.057	11.4	0.995
	0.50	0.05	0.001	5.23	0.848
	0.50	0.10	0.108	1.18	0.993
	0.50	0.60	0.309	1.30	0.992
	1.0	0.05	0.029	1.71	0.977
	1.0	0.10	0.050	1.64	0.987
	1.0	0.60	0.279	1.50	0.995
Clark	C_0 (mM)	Q (mL min^{-1})	k_C	A	R^2
	0.25	0.05	0.033	1.37E+32	0.993
	0.25	0.10	0.020	2.68E+9	0.906
	0.25	0.60	0.301	2.6E+22	0.995
	0.50	0.05	0.001	21.0	0.848
	0.50	0.10	0.113	2.3E+26	0.993
	0.50	0.60	0.327	8.1E+13	0.992
	1.0	0.05	0.061	4.64E+20	0.977
	1.0	0.10	0.106	1.37E+17	0.988
	1.0	0.60	0.583	2.34E+14	0.9955
Yoon-Nelson	C_0 (mM)	Q (mL min^{-1})	k_{YN} (min^{-1})	τ (min)	R^2
	0.25	0.05	0.012	226,7	0.989
	0.25	0.10	0.012	103,8	0.914
	0.25	0.60	0.155	170	0.996
	0.50	0.05	0.001	263,3	0.848
	0.50	0.10	0.056	5331	0.992
	0.50	0.60	0.173	95.8	0.993
	1.0	0.05	0.031	768	0.974
	1.0	0.10	0.055	367	0.992
	1.0	0.60	0.293	56.0	0.996
Yan	C_0 (mM)	Q (mL min^{-1})	k_{Yan}	Q_e (mM g^{-1})	R^2
	0.25	0.05	4.65	20.4	0.991
	0.25	0.10	4.45	10.7	0.913
	0.25	0.60	56.4	22.9	0.995
	0.50	0.05	0.107	0.40	0.850
	0.50	0.10	5.17	24.0	0.989
	0.50	0.60	17.0	12.2	0.990
	1.0	0.05	1.03	13.2	0.970
	1.0	0.10	1.74	11.8	0.993
	1.0	0.60	7.88	9.55	0.994

results (Fig. 4b) show that P sorption is best modeled by pseudo second-order kinetics, indicating a strong chemical sorption of P to FGD gypsum. The batch sorption experiments were satisfactorily modeled by the Freundlich sorption isotherm, suggesting multilayer sorption onto FGD gypsum surface. This further implies that sorbed P molecules interact on the surface and form a multilayer of sorbed P. Additionally, batch sorption experiments produced a Q_{max} value of 36.1 mM kg^{-1} at the equilibrium time of 24 h. Langmuir and Freundlich modeling and production of this Q_{max} value is consistent with the findings from kinetics experiments, since the highest sorbed amount of 35.7 mM kg^{-1} was reached at 24 h for initial P concentration of 0.25 mM. The fixed-bed column experiments showed that sorption rate is directly proportional to flow rate, but irrespective of initial P concentration. It also determined earlier breakthrough at higher flow rate and higher initial P concentration. This is consistent with findings from kinetics experiments since the boundary layer diffusion and intraparticle diffusion steps were faster at higher initial P concentrations.

The complementary findings of P sorption by FGD gypsum from the kinetics, batch sorption, and fix-bed column experiments advance our understanding of P sorption rate, time required for reaching maximum sorption, and potential saturation time of FGD gypsum under different initial P concentrations and flow rates. These findings can be further extrapolated to understand at what time point an FGD gypsum filter would need to be replaced based on wastewater (or manure/fertilizer contaminated runoff) volume, flow rate, and initial P concentration through the filter. The data can also be utilized in water bodies, since it will be apparent what amount of FGD gypsum would need to be utilized based on water volume and initial P concentration in the waterbody. Kinetics, batch sorption, or fixed-bed column experiments alone would have been unable to provide the comprehensive outlook on the efficiency of FGD gypsum to sorb P for various conditions and goals.

4. Conclusion

The FGD gypsum is a waste byproduct from coal-powered energy plants with a high purity of gypsum (99.6%). The FGD gypsum provides a physiochemical approach for P remediation in waters via physical and chemical sorption. The equilibrium of P sorption by the FGD gypsum was reached at 24 h, with a two-step (fast sorption and slow intraparticle diffusion reaction rate) sorption process. The sorption kinetics is best modeled by pseudo second-order kinetics model, suggesting that chemical reactions dominate the interactions between gypsum and P. The FGD gypsum can remove 14.3% and 82.1% of the P at various P concentrations evaluated (0.01–0.25 mM). The sorption isotherm is best modeled by the Freundlich model, suggesting multilayer sorption. The fixed-bed column breakthrough experiments showed that there is an earlier P breakthrough across pore volumes at higher flow rate conditions under higher initial P concentrations. The column breakthrough curve slope is largely depended on both initial P concentration and flow rate, due to the faster sorption kinetics of P by FGD gypsum. Column sorption modeling results indicate sorption rate is positively correlated with flow rate, while independent on the initial P concentration. Our findings clearly indicate the FGD gypsum has the capacity to remove P under a wide range of concentrations from water. These findings can be further extrapolated to develop gypsum-enabled water treatment techniques. These include direct addition to aquaculture ponds and standing water bodies, gypsum-bed filtration and trenches for runoff, or wastewater drainage filtration. Further research is needed to investigate the use of FGD gypsum in large-scale practical applications and associated costs and longevity (e.g., gypsum packed bed).

Author contributions statement

Ansley Hamid: Data acquisition and analysis, original draft preparation, and revision. **Alan E. Wilson**: Conceptualization and writing – review and editing. **H. Allen Torbert**: Conceptualization and writing – review and editing. **Dengjun Wang**: Project administration, conceptualization, methodology, and writing – review and editing.

Declaration of competing interest

The authors declare that they have no known competing financial interests or personal relationships that could have appeared to influence the work reported in this paper.

Data availability

Data will be made available on request.

Acknowledgments

This research was supported by the U.S. Department of Agriculture

(USDA), National Institute of Food and Agriculture (NIFA), Hatch Program, Alabama Agricultural Experiment Station (ALA016-1-19123, to D. W.) and the USDA Agricultural Research Service (ARS) under Agreement No. 58-6010-0-006 (to H.T.).

Appendix A. Supplementary data

Supplementary data to this article can be found online at https://doi.org/10.1016/j.chemosphere.2023.138062.

References

Ahmad, A.A., Hameed, B.H., 2010. Fixed-bed adsorption of reactive azo dye onto granular activated carbon prepared from waste. J. Hazard Mater. 175 (1–3), 298–303.

Bastin, O., et al., 1999. Phosphorus removal by a synthetic iron oxide–gypsum compound. Ecol. Eng. 12 (3–4), 339–351.

Bohart, G.S., Adams, E.Q., 1920. Some aspects of the behavior of charcoal with respect to chlorine. J. Am. Chem. Soc. 42 (3), 523–544.

Boyd, C.E., Tucker, C.S., 2012. Pond Aquaculture Water Quality Management. Springer Science & Business Media.

Bryant, R.B., et al., 2012. Using flue gas desulfurization gypsum to remove dissolved phosphorus from agricultural drainage waters. J. Environ. Qual. 41 (3), 664–671.

Buley, R.P., et al., 2021. Field evaluation of seven products to control cyanobacterial blooms in aquaculture. Environ. Sci. Pollut. Control Ser. 28 (23), 29971–29983.

Cavalcante, C.L., 2000. Industrial adsorption separation processes: fundamentals, modeling and applications. Lat. Am. Appl. Res. 30 (4), 357–364.

Chakrabarti, S., 2018. Eutrophication—a global aquatic environmental problem: a review. Res. Rev.: Ecol. Environ. Sci. 6, 1–6.

Chen, L., Warren, D., 2011. Gypsum as an Agricultural Amendment. Ohio State University.

Cheng, P., et al., 2018. Enhanced adsorption capacity for phosphate in wastewater from thermally activated flue gas desulfurization gypsum. J. Chem. Technol. Biotechnol. 93 (6), 1733–1741.

Chiavola, A., D'Amato, E., Baciocchi, R., 2012. Ion exchange treatment of groundwater contaminated by arsenic in the presence of sulphate. Breakthrough experiments and modeling. Water, Air, Soil Pollut. 223 (5), 2373–2386.

Chislock, M., et al., 2013. Eutrophication: causes, consequences, and controls in aquatic ecosystems. Nat. Educ. Knowl. 4 (4), 10.

Clark, R.M., 1987. Evaluating the cost and performance of field-scale granular activated carbon systems. Environ. Sci. Technol. 21 (6), 573–580.

Crangle, R.D., 2021. Gypsum Translated by Mineral Commodity Summaries. U.S. Geological Society.

de Franco, M.A.E., 2017. Removal of amoxicillin from water by adsorption onto activated carbon in batch process and fixed bed column: kinetics, isotherms, experimental design and breakthrough curves modelling. J. Clean. Prod. 161, 947–956.

Dodds, W.K., et al., 2009. Eutrophication of US freshwaters: analysis of potential economic damages. Environ. Sci. Technol. 43 (1), 12–19.

Dontsova, K., et al., 2005. Gypsum for Agr Ohio—Sources and Quality of Available Products. Ohio State University.

Egle, L., Rechberger, H., Zessner, M., 2015. Overview and description of technologies for recovering phosphorus from municipal wastewater. Resour. Conserv. Recycl. 105, 325–346.

Gypsum Association, 2022. FGD Gypsum Production Process. Gypsum Association. In: https://gypsum.org/fgd-gypsum-production-process/.

He, K., Li, X., Dong, L., 2018. The effects of flue gas desulfurization gypsum (FGD gypsum) on P fractions in a coastal plain soil. J. Soils Sediments 18, 804–815.

Higgins, B.P.J., Mohleji, S.C., Irvine, R.L., 1976. Lake treatment with fly ash, lime, and gypsum. J. (Water Pollut. Contr. Federat.) 48 (9), 2153–2164.

Huang, J., et al., 2022. Fixed bed column performance of Al-modified biochar for the removal of sulfamethoxazole and sulfapyridine antibiotics from wastewater. Chemosphere 305, 135475.

Johansson, L., 1999. Industrial by-products and natural substrata as phosphorus sorbents. Environ. Technol. 20 (3), 309–316.

Kamitsou, M.D., et al., 2020. Valorization of FGD and bauxite residue in sulfobelite cement production. Waste Biomass Valor. 11 (10), 5445–5456.

Klimeski, A., Uusitalo, R., Turtola, E., 2014. Screening of Ca-and Fe-rich materials for their applicability as phosphate-retaining filters. Ecol. Eng. 68, 143–154.

Komiyama, T., Ito, T., 2019. The characteristics of phosphorus in animal manure composts. Soil Sci. Plant Nutr. 65 (3), 281–288.

Kordlaghari, M.P., Rowell, D.L., 2006. The role of gypsum in the reactions of phosphate with soils. Geoderma 132 (1–2), 105–115.

Koukouzas, N., Vasilatos, C., 2008. Mineralogical and chemical properties of FGD gypsum from Florina, Greece. J. Chem. Technol. Biotechnol. 83 (1), 20–26.

Lehtiniemi, M., Engström-Öst, J., Viitasalo, M., 2005. Turbidity decreases anti-predator behaviour in pike larvae, *Esox lucius*. Environ. Biol. Fish. 73 (1), 1–8.

Lengnick, L., 2014. Resilient Agriculture: Cultivating Food Systems for a Changing Climate. New Society Publishers, p. 288.

Ma, H., Khalaf, A., Chen, R., Wang, Z., Li, Y., Xu, F., 2023. Evaluation of flue gas desulfurization gypsum as a low-cost precipitant for phosphorus removal from anaerobic digestion effluent filtrate. IOP Conf. Ser. Earth Environ. Sci. 1135 (1), 012011.

Murphy, J., Riley, J.P., 1962. A modified single solution method for the determination of phosphate in natural waters. Anal. Chim. Acta 27, 31–36.

Newswire, C.D.N., 2022. Flue gas desulfurization (FGD) gypsum market: CAGR analysis, product supply and demand, sales volume by product types, key players and applications. Digit. J. 17 Feb https://www.digitaljournal.com/pr/flue-gas-desulfurization-fgd-gypsum-market-cagr-analysis-product-supply-and-demand-sales-volume-by-product-types-key-players-and-applications.

Patel, H., 2019. Fixed-bed column adsorption study: a comprehensive review. Appl. Water Sci. 9 (3), 1–17.

Redfield, A.C., 1958. The biological control of chemical factors in the environment. Am. Sci. 46 (3), 221, 230A.

Sheng, L., et al., 2018. Mesoporous/microporous silica materials: preparation from natural sands and highly efficient fixed-bed adsorption of methylene blue in wastewater. Microporous Mesoporous Mater. 257, 9–18.

Thomas, H.C., 1944. Heterogeneous ion exchange in a flowing system. J. Am. Chem. Soc. 66 (10), 1664–1666.

Torbert, H.A., Watts, D.B., 2014. Impact of flue gas desulfurization gypsum application on water quality in a coastal plain soil. J. Environ. Qual. 43 (1), 273–280.

U.S. EPA, 1983. Control of Organic Substances in Water and Wastewater. United States Environmental Protection Agency. EPA600/8-83-011.

U.S. EPA, 2008. Agricultural Uses for Flue Gas Desulfurization (FGD) Gypsum. United States Environmental Protection Agency. EPA530-F-08-009.

Van Donk, E., et al., 1990. Whole-lake food-web manipulation as a means to study community interactions in a small ecosystem. Hydrobiologia 200, 275–289.

Wang, J., Zhang, Y., Feng, C., Li, J., Li, G., 2009. Adsorption capacity for phosphorus comparison among activated alumina, silica sand and anthracite coal. J. Water Resour. Protect. 4, 260–264.

Wang, D.J., Jin, Y., Jaisi, D.P., 2015. Effect of size-selective retention on the cotransport of hydroxyapatite and goethite nanoparticles in saturated porous media. Environ. Sci. Technol. 49 (14), 8461–8470.

Wang, D.J., Park, C.M., Masud, A., Aich, N., Su, C., 2017. Carboxymethylcellulose mediates the transport of carbon nanotube—magnetite nanohybrid aggregates in water-saturated porous media. Environ. Sci. Technol. 51 (21), 12405–12415.

Wang, D.J., Jin, Y., Park, C.M., Heo, J., Bai, X., Aich, N., Su, C., 2018. Modeling the transport of the "new-horizon" reduced graphene oxide—metal oxide nanohybrids in water-saturated porous media. Environ. Sci. Technol. 52 (8), 4610–4622.

Watts, D.B., Dick, W.A., 2014. Sustainable uses of FGD gypsum in agricultural systems: introduction. J. Environ. Qual. 43 (1), 246–252.

Weber, W.J., Morris, J.C., 1963. Kinetics of adsorption on carbon from solution. J. Sanit. Eng. Div. 89 (2), 31–59.

Wu, R., Boyd, C.E., 1990. Evaluation of calcium sulfate for use in aquaculture ponds. Progress. Fish Cult. 52 (1), 26–31.

Yan, G., Viraraghavan, T., Chen, M., 2001. A new model for heavy metal removal in a biosorption column. Adsorpt. Sci. Technol. 19 (1), 25–43.

Yoon, Y.H., Nelson, J.H., 1984. Application of gas adsorption kinetics I. A theoretical model for respirator cartridge service life. Am. Ind. Hyg. Assoc. J. 45 (8), 509–516.

Zhang, W., et al., 2011. Removal of methylene blue from aqueous solutions by straw based adsorbent in a fixed-bed column. Chem. Eng. J. 173 (2), 429–436.

Zhang, B., Li, J., Li, Y., Li, H., 2018. Adsorption characteristics of several bioretention-modified fillers for phosphorus. Water 10 (7), 831.

Zhang, Y., et al., 2020. Control and remediation methods for eutrophic lakes in the past 30 years. Water Sci. Technol. 81 (6), 1099–1113.